Intraconfiguration interactions in barium $6p_{1/2}nf$ autoionizing states

X. Wang, J. G. Story, and W. E. Cooke
Department of Physics, University of Southern California, Los Angeles, California 90089-0484
(Received 4 October 1990)

Measurements are reported of the energies and linewidths of the $J=2$, 3, and 4 components of the $6p_{1/2}14f$ and $6p_{1/2}19f$ states of barium. These states are anomalously broad, having autoionization lifetimes of approximately $\frac{1}{2}$ of a classical Rydberg orbit period, and previously measurements have discerned no differences among the various J components. This work shows that the differences can be observed, and are consistent with calculations. The variations between states would be large if the states were LS coupled, but the large $6p$ ionic fine-structure forces recoupling into jj configurations. The spherical symmetry of the $6p_{1/2}$ ionic state minimizes the differences between J states, but does not eliminate them.

I. INTRODUCTION

Over the last decade, the isolated core excitation[1] (ICE) method has produced an abundance of spectroscopic information about doubly excited states of alkaline-earth atoms.[2,3] *Ab initio* calculations,[4,5] using a multichannel quantum-defect theory (MQDT) formalism,[6-9] have produced good agreement with many of the measured characteristics, including excitation energies,[5] linewidths,[10] and branching ratios into final continuum channels.[11] The calculations begin with a basis set of channels having prescribed angular momentum J and parity, including all possible inner- and outer-electron quantum numbers consistent with those prescriptions. Since all internal interactions conserve both parity and total angular momentum, it is natural to separate states according to this classification. However, the ICE measurements have illustrated that most of the doubly excited states (with the inner electron not excited too far beyond its valence state) are composed primarily of a single, $mlnl'$ configuration. In fact, the ICE measurements usually excite several different J states within the $mlnl'$ multiplet, and surprisingly, the multiplet often appears as a single line, with the different J states all having very similar characteristics.[3,12-15]

In this paper, we have studied the $6p_{1/2}nf$ states of barium for several values of n, using the ICE technique. We have found that all four states which we excited ($J=$ 2, 3, 3, and 4) had very similar energies and autoionization-induced linewidths. This is consistent with the work of other groups which have found no discernable difference between excitation spectra taken with different excitation polarizations.[14,15] These states have anomalously large autoionization rates, with decay times of approximately $\frac{1}{2}$ of the classical orbit period. We have analyzed these states using a single configuration to calculate their energy splittings, and their linewidths due to autoionization to the various allowed continua. We find only two continua are responsible for these anomalously large decay rates — the $6s\epsilon g$ and the $5d\epsilon g$. Although this seems to suggest that large variations should occur in the decay rates of the various J states, we find that the isotropic nature of the $6p_{1/2}$ ion core state (after allowing for the large core fine structure) mixes the LS states together to obscure these differences. Even in the case of the two nearly degenerate $J=3$ states, where the states would be expected to recouple to maximize the difference between their linewidths, we find that the two states have linewidths within 30% of each other, and that there will be no evidence for interference between them, when the ICE method is used to excite them. Nevertheless, by using well-controlled laser polarizations for our excitations, we are able to see remnants of the large differences between the contributions of different LS configurations to autoionization, without a state selective detection technique.

II. EXPERIMENT

The basic idea of the ICE technique is to excite a two-electron transition in several steps, so that only one electron is excited during each step. The interaction between the electrons then does not affect the transition moments to produce complicated line shapes, but instead only broadens and shifts the final states' energies. Usually, ICE spectra have a high degree of symmetry, or very high Fano q parameters,[16] so that the line shapes can be treated as simple Lorentzian lines. Moreover, the ICE method usually excites only a single, well-defined configuration, so that the transition *strengths* are also understood in detail. For those few cases where no well-defined dominant configuration exists, the ICE method

shows this unambiguously, since the line shapes deviate significantly from the usual simple, high-q cases.[17] The ICE method therefore presents a clean way to excite and to characterize a doubly excited atomic state.

For these experiments we have used a four-step laser excitation scheme, with the first three steps exciting the outer, or Rydberg, electron to an nf state, and a final laser exciting the inner core electron to a $6p$ state. To do this, we crossed an effusive atomic beam of barium atoms with four lasers as shown in Fig. 1 to produce $6p_{1/2}nf$ states. Two dye lasers and a fixed frequency 1.06-μm neodymium-doped yttrium-aluminum-garnet (Nd:YAG) laser first excited the nf Rydberg electron as shown in Fig. 2. The first dye laser, at 481 nm, and the 1.064-μm laser excited the $6s5d\,^1D_2$ state through stimulated Raman scattering. These two lasers were polarized linearly, and parallel, so that only the $m_J = 0$ state was populated. This stimulated excitation has an advantage over nonstimulated excitation methods, such as cascade pumping[14] or discharge pumping,[15] because the $6s5d\,^1D_2$ state can be *completely* characterized in all of its quantum numbers. A frequency-doubled dye laser, at approximately 330 nm (depending on the n state to be populated) drove the next excitation step, $6s5d \rightarrow 6snf$, again linearly polarized parallel to the first two lasers, so that the final Rydberg state was a $6snf\,^1F_3$ with a magnetic quantum number of $m_J = 0$. With such a well-defined Rydberg state, the core transition, $6snf \rightarrow 6p_{1/2}nf$, can only produce transitions to well-defined J, m_J states, thereby allowing us to observe the small differences between the spectra of the different J states.

The first dye laser was pumped by the third harmonic of the same Nd:YAG laser, while the second two dye lasers were pumped by the third harmonic of a second Nd:YAG laser, triggered some 20 ns later. In addition, an optical delay of approximately 10 ns insured that the third dye laser arrived after the excitation to the Rydberg state was completed. All of the dye lasers had pulse lengths of approximately 5 ns, while the Nd:YAG pulse lengths were approximately 10 ns. All of the dye lasers had linewidths of 0.3–0.5 cm^{-1}. The excitation region was between two parallel capacitor plates, which were biased with a small voltage (10 V/cm) to force the autoionization-produced ions through a shielding screen into a microchannel plate particle multiplier. A microcomputer recorded this ion signal after several shots were averaged by a boxcar integrator, and swept the wavelength of the final core laser to produce an excitation spectra.

Several independent profiles were taken on each of several days for each polarization condition and each of the two $6p_{1/2}nf$ configurations ($n = 14$ and 19). A spectrum typically consisted of 200 data points, each averaged over 10 ($n = 14$) or 50 ($n = 19$) laser shots, so that an entire spectrum required 5 minutes ($n = 14$) or 20 minutes ($n = 19$). We then summed several of these short frequency sweeps, rather than average each data point for a longer time, to reduce the effects of long term laser power drifts. Similar spectra were obtained on seven different days, although because we suffered small variations in the laser power profile (due to decaying dye) and in the laser frequency offset, we have not usually added together the spectra from different days.

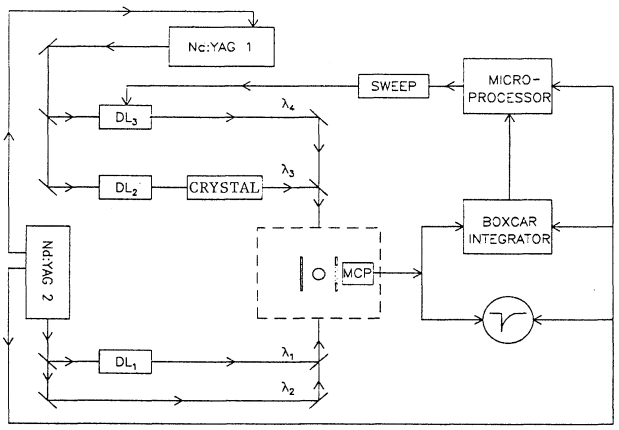

FIG. 1. Schematic diagram of the apparatus.

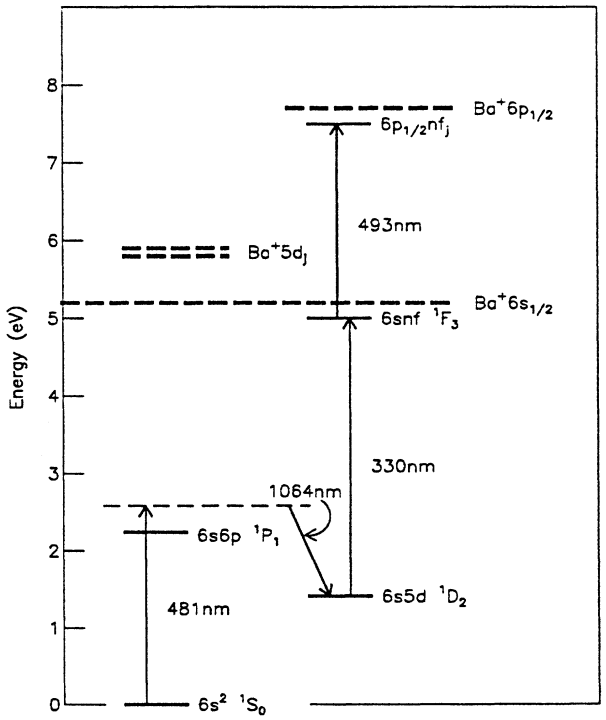

FIG. 2. Energy-level diagram of barium.

TABLE I. Relative excitation strengths of the different J states with the core laser polarization parallel (||) or perpendicular ($\perp$) to the other three excitation lasers' polarizations.

J	2	3	4
||	6	0	8
$\perp$	2	7	5

The major advantage of using four excitation lasers is that every step proceeds with a very-well-defined polarization, so that the final-state excitation can be well defined. Consequently, it is also important to maintain that polarization throughout the entire excitation process. To insure this, we varied the small collection voltage between 1 and 100 V/cm, with no effect on the spectra. We also varied the time delay between the two Nd:YAG lasers from $\approx$1 to 500 ns, to check for depolarizations in the $6snf$ Rydberg state, and again detected no changes in the excitation spectra. As a result of this careful control of the excitation process, we obtained two distinct types of excitation spectra. When the core laser polarization was parallel (||) to that of the first two lasers, we excited *only* $J = 2$ or 4 states. When the core laser polarization was perpendicular to that of the first three lasers, ($\perp$), 50% of the excitation went into the $J = 3$ states. The details of the relative populations are listed in Table I.

III. THEORY

A doubly excited state is most conveniently described by the sum of the spins of the two electrons, $\mathbf{S} = \mathbf{s}_1 + \mathbf{s}_2$, and by the sum of their orbital angular momenta, $\mathbf{L} = \mathbf{l}_1 + \mathbf{l}_2$, since the electrostatic interaction is diagonal with respect to both of these quantities. However, the large fine structure of the $6p$ ionic core of barium forces the states into eigenstates in which the inner electron's spin and angular momentum are coupled to make a core j_1. Nevertheless, it is far easier to begin any calculations from an LS coupled basis, and to make the transformation to a jj or jl basis only as a final step. Thus, a $6pnf$ state can occur in the $^{1,3}D$, $^{1,3}F$, and $^{1,3}G$ configurations. The energies of these configurations are separated by the direct quadrupole F^2, exchange quadrupole G^2, and exchange hexadecapole G^4 interactions since only these will conserve parity and obey the angular momentum triangle sum rule. Following Sobelman,[18] we have written the energy shifts of these configurations as

$$\begin{aligned} E(^{1,3}D) &= \tfrac{4}{25}F^2 \pm \tfrac{3}{175}G^2 \pm \tfrac{4}{21}G^4 , \\ E(^{1,3}F) &= -\tfrac{1}{5}F^2 \mp \tfrac{3}{35}G^2 \pm \tfrac{1}{21}G^4 , \\ E(^{1,3}G) &= \tfrac{1}{15}F^2 \pm \tfrac{9}{35}G^2 \pm \tfrac{1}{189}G^4 , \end{aligned} \tag{1}$$

where the upper sign is used for singlet states and the lower sign is used for triplet states. The direct and exchange interactions are defined as

$$F^k = \int \frac{r_<^k}{r_>^{k+1}} R^2_{n_1 l_1}(r_1) R^2_{n_2 l_2}(r_2) r_1^2 dr_1 r_2^2 dr_2$$

$$G^k = \int \frac{r_<^k}{r_>^{k+1}} R_{n_1 l_1}(r_1) R_{n_2 l_2}(r_1) R_{n_1 l_1}(r_2) R_{n_2 l_2}(r_2) r_1^2 dr_1 r_2^2 dr_2 . \tag{2}$$

Both L and S are also conserved during autoionization, so that the available continua are different for each of these configurations:

$^{1,3}D$: $6s\epsilon d$, $5d\epsilon s$, $5d\epsilon d$, $5d\epsilon g$,

$^{1,3}F$: $5d\epsilon d$, $5d\epsilon g$,

$^{1,3}G$: $6s\epsilon g$, $5d\epsilon d$, $5d\epsilon g$.

[We have ignored the $5d\epsilon(l = 6)$ continuum since its very high angular momentum value pushes the outer electron far from the core, making the radial integrals much smaller than those for which the outer l only changes by 1.] The matrix element that causes autoionization may be written as

$$\left\langle n_1 l_1, n_2 l_2 SL \left| \frac{1}{r_{12}} \right| n_3 l_3, n_4 l_4 SL \right\rangle = \sum_k [\alpha_k R^d_k + (-1)^S \beta_k R^e_k] , \tag{3}$$

where the two-electron integrals R_k are defined as the direct and exchange integrals of multipole interactions:

$$R^d_k = \int \frac{r_<^k}{r_>^{k+1}} R_{n_1 l_1}(r_1) R_{n_3 l_3}(r_1) R_{n_2 l_2}(r_2) R_{n_4 l_4}(r_2) r_1^2 dr_1 r_2^2 dr_2$$

$$R^e_k = \int \frac{r_<^k}{r_>^{k+1}} R_{n_1 l_1}(r_1) R_{n_4 l_4}(r_1) R_{n_2 l_2}(r_2) R_{n_3 l_3}(r_2) r_1^2 dr_1 r_2^2 dr_2 . \tag{4}$$

TABLE II. Angular factors for the configuration mixing of $6pnf$ states with the various continua into which they may autoionize.

$nl\epsilon l'$	α_1	β_1	α_3	β_3	β_5	L
$6s\epsilon d$	-0.447			-0.192		2
$6s\epsilon g$	0.385			0.165		4
$5d\epsilon s$		-0.447	-0.192			2
	0.107	0.107	0.183	0.183		2
$5d\epsilon d$	0.239	-0.239	-0.102	0.102		3
	0.414	0.414	0.020	0.020		4
	-0.478		-0.102	-0.022	-0.181	2
$5d\epsilon g$	-0.378		0.162	0.090	-0.057	3
	-0.241		-0.085	-0.172	-0.010	4

Here, the geometric coefficients α_k and β_k can be derived from 6-j symbols and reduced matrix elements as

$$\alpha_k = \langle l_1(1) l_2(2) L M_L | P_k(\cos\theta) | l_3(1) l_4(2) L M_L \rangle = (-1)^{l_2+l_3+L} (l_1 \| C^k \| l_3)(l_2 \| C^k \| l_4) \begin{Bmatrix} l_1 & l_2 & L \\ l_4 & l_3 & k \end{Bmatrix} , \tag{5}$$

$$\beta_k = \langle l_1(1) l_2(2) L M_L | P_k(\cos\theta) | l_3(2) l_4(1) L M_L \rangle = (-1)^{l_1+l_4} (l_1 \| C^k \| l_4)(l_2 \| C^k \| l_4) \begin{Bmatrix} l_1 & l_2 & L \\ l_3 & l_4 & k \end{Bmatrix} .$$

These angular factors are summarized in Table II, while the radial matrix elements are summarized in Table III.

To obtain the radial matrix elements of Table III, we constructed two-electron wave functions, by first calculating single-electron ionic core wave functions, representing the Xe-like hard core with a model potential. The model potential was a Gaussian charge distribution of the 54 core electrons, with a radius chosen to give the correct ionic quantum defect. Since most of the nf Rydberg wave function lies outside this hard core, the details of it were relatively unimportant to the calculation. After this, we froze the inner-electron wave function and calculated the Rydberg electron wave function, using the hard core and the added charge distribution of the first electron. In those cases where the ionic electron and the Rydberg electron had the same l value, we added a Lagrangian multiplier to insure that the two radial wave functions were orthogonal. For bound and free Rydberg electrons, we normalized the wave functions per unit energy. This means that a bound Rydberg wave function will be normalized to $(n^*)^3$, while a continuum radial wave function will have the asymptotic form,[19] when averaged over its oscillations:

$$|R|^2 \rightarrow \frac{1}{\pi k r^2} . \tag{6}$$

This form is only valid for $E = k^2/2 >> 1/r$, and we typically applied it for r values larger than 400 a.u.

The autoionization rate of a specific LS configuration can be obtained from Fermi's golden rule by first summing all the matrix elements leading to a given continuum and then squaring and summing over all continuum channels:

$$A_S = 2\pi \sum_{\{\epsilon\}} \left(\sum_k [\alpha_k R_k^d + (-1)^S \beta_k R_k^e] \right)^2 . \tag{7}$$

These products and the autoionization rate for each configuration is summarized in Table IV.

From Table IV, a few generalizations are clear. The most important decay routes lead to a ϵg continuum electron, and spin effects are unimportant for these channels. The large contribution of the l_2+1 decay route has been noted by Jones and Gallagher in their calculations of the decay rates for high-l_2 states.[20] This tendency should be expected generally for dipole allowed autoionization. To the extent that the Coulomb interaction is separable, the dipole expansion term (which has the same form as the angular momentum potential barrier) is proportional to the wave-function overlap:

$$\left\langle nl \left| \frac{1}{r^2} \right| \epsilon l' \right\rangle = \frac{\langle nl | \epsilon l' \rangle}{l_>} . \tag{8}$$

Although this proportionality will not be true in general, nevertheless, the overlap between the initial and final wave functions will still be an important measure of the autoionization magnitude. This overlap will be determined primarily by the location of the *inner radial*

TABLE III. Direct and exchange integrals leading to the autoionization of the $6pnf$ states of barium.

$nl\epsilon l'$	k	R_k^d	R_k^e
$6s\epsilon d$	1	0.210	
	3		0.178
$6s\epsilon g$	1	-0.560	
	3		-0.166
$5d\epsilon s$	1		-0.017
	3	0.028	
$5d\epsilon d$	1	0.171	0.171
	3	0.123	0.103
$5d\epsilon g$	1	-0.319	
	3	-0.126	-0.072
	5		-0.048

TABLE IV. The autoionization matrix elements and decay rates for each LS configuration of the $6pnf$ states.

L	$nl\epsilon l'$	$\alpha_1 R_1^d$	$\beta_1 R_1^e$	$\alpha_3 R_3^d$	$\beta_3 R_3^e$	$\beta_5 R_5^e$	$A_{S=0}$	$A_{S=1}$
2	$5d\epsilon g$	0.1525		0.0129	0.0017	0.0087	0.19	0.15
	$6s\epsilon d$	-0.0939			-0.0342		0.10	0.02
	$5d\epsilon d$	0.0183	0.0183	0.0225	0.0188		0.04	0.00
	$5d\epsilon s$		0.0076	-0.0054			0.00	0.00
						Total:	0.33	0.17
3	$5d\epsilon g$	0.1206		-0.0204	-0.0065	0.0027	0.06	0.07
	$5d\epsilon d$	0.0409	-0.0409	-0.0125	0.0105		0.00	0.02
						Total:	0.06	0.09
4	$6s\epsilon g$	-0.2156			-0.0274		0.37	0.22
	$5d\epsilon d$	0.0708	0.0708	0.0025	0.0021		0.13	0.00
	$5d\epsilon g$	0.0769		0.0107	0.0124	0.0005	0.06	0.04
						Total:	0.57	0.26

turning points of the two wave functions. The continuum $l+1$ channel has its inner turning point pushed out by its higher l value, but simultaneously pulled in by the increased energy of the continuum electron. For the $6p_{1/2}19f \rightarrow 6s\epsilon g$ case, the initial energy is -38 meV, while the final energy is +2.47 eV.

Since the autoionization matrix element is primarily determined by the overlap of inner turning points of the initial and final Rydberg wave functions, one might expect the autoionization rates to decrease monotonically with increasing l. Although this is true for high l states,[20] both barium and strontium have their largest rates occuring for the nf states. As was pointed out by Jones and Gallagher,[20] this is because the nf states are the first states to have nearly hydrogenic wave functions. Since the lower l states penetrate the core, their turning points are pulled in to radii much smaller than the hydrogenic values. The ratio of the interelectron interaction to the binding potential *decreases* since the high-Z core becomes unshielded. In a calculation this effect shows up as an interference between the initial and final wave functions which tends to cancel the autoionization matrix element.

The F configurations decay much more slowly than either D or G configurations because the F configurations have no $6s$ ion core decay channel which conserves parity. They may autoionize to the $5d\epsilon g$ channel, and Table IV shows that this is the largest term. However, this is partially cancelled by the octupole coupling to that same final channel, so the effect is reduced. This reduction by a higher-order multipole will generally occur for those intial configurations where the pl electrons couple to make $L=l$. Such configurations correspond to classical "out-of-plane" orbits, where one would expect reduced classical autoionization collisions. Since the α_i coeffficients are generally monotonic in L, this classical effect can only arise through the cancellation of many multipole moments, which will be present in the nearly classical limit of both electrons having high-l values. But, even for our case of small core l, we generally expect states with $L=l_2$ to live the longest of the $6pnl_2$ configurations.

However, the large fine structure in the $Ba^+ 6p$ ion core forces the states to recouple into states with $\mathbf{j}_1 = \boldsymbol{l}_1 + \mathbf{s}_1$ conserved. If we begin with a jj-coupled basis, and we restrict ourselves to considering the $6p_{1/2}$ states, then the states may be written as

$$
\begin{aligned}
(\tfrac{1}{2}\tfrac{5}{2})_2 &= +0.577\ {}^1D - 0.471\ {}^3D + 0.667\ {}^3F\ , \\
(\tfrac{1}{2}\tfrac{5}{2})_3 &= -0.106\ {}^3D + 0.436\ {}^1F - 0.252\ {}^3F + 0.857\ {}^3G\ , \\
(\tfrac{1}{2}\tfrac{7}{2})_3 &= -0.738\ {}^3D + 0.378\ {}^1F + 0.546\ {}^3F - 0.124\ {}^3G\ , \\
(\tfrac{1}{2}\tfrac{7}{2})_4 &= -0.500\ {}^3F + 0.577\ {}^1G + 0.646\ {}^3G\ .
\end{aligned}
\tag{9}
$$

This simplifies the energies considerably, since the $6p_{1/2}$ ion core has no electric multipole moments at all. Consequently, the *only* terms which split the states are *exchange* quadrupole and exchange hexadecapole terms:

$$
\begin{aligned}
\Delta E[(\tfrac{1}{2}\tfrac{5}{2})_{J=2}] &= +\tfrac{1}{25}G^2\ , \\
\Delta E[(\tfrac{1}{2}\tfrac{5}{2})_{J=3}] &= -\tfrac{1}{81}G^4\ , \\
\Delta E[(\tfrac{1}{2}\tfrac{7}{2})_{J=3}] &= -\tfrac{1}{5}G^2\ , \\
\Delta E[(\tfrac{1}{2}\tfrac{7}{2})_{J=4}] &= -\tfrac{1}{9}G^4\ .
\end{aligned}
\tag{10}
$$

In view of the large linewidths of the $6pnf$ states, we will ignore all of the exchange terms and treat these states as degenerate. (Our spectra typically have several lines, separated by less than their linewidths.) This will also hold true, in general, for most other $6p_{1/2}nl$ states.[3,12,13]

Given the transformation matrix of Eq. (3), and the rates of Table IV, we can now calculate the linewidths of the $(6p_{\frac{1}{2}}nf_j)_J$ states. Table V lists the width(Γ) of each $(6p_{\frac{1}{2}}nf_j)_J$ state and the contributions of each LS channel to the width. The two $J=3$ states should first be recoupled to orthogonalize their autoionization continua (since the two states are nearly diagonal). However, the

jj-coupling scheme almost accomplishes this by itself (as can be seen from Table V), so we have left the states as jj coupled for simplicity. Notice that after recoupling, the linewidths of the $J = 3$ states are almost as broad as the $J = 2$ state. In general, the maximum and minimum linewidths will be closer to the average linewdth after the states are recoupled from an LS basis to a jj basis.

Since the core transition conserves electronic spin, and the initial states have primarily singlet character, only the singlet character in the final $(6p_{\frac{1}{2}}nf_j)_J$ states is excited. Using the ICE model, the core transition can thus be written as

TABLE V. The contributions of each LS channel to the calculated widths of the $6p_{1/2}nf$ states.

jj	Γ	^1D	^3D	^1F	^3F	^1G	^3G
$\frac{1}{2}\frac{5}{2}, J=2$	0.19	58%	20%		22%		
$\frac{1}{2}\frac{5}{2}, J=3$	0.21		1%	5%	3%		91%
$\frac{1}{2}\frac{7}{2}, J=3$	0.13		70%	7%	20%		3%
$\frac{1}{2}\frac{7}{2}, J=4$	0.31				7%	59%	34%

$$\langle 6snf\ ^1F_3(M)|\boldsymbol{\mu}_1\cdot\mathbf{E}|6pn'f\ ^1L_{J=L}(M')\rangle = \begin{pmatrix} 1 & 3 & L \\ -m_1 & -m_2 & M' \end{pmatrix} \langle 6s|\boldsymbol{\mu}_1\cdot\mathbf{E}|6p\rangle\langle nf|n'f\rangle\ , \tag{11}$$

where $\langle nf|n'f\rangle$ is the overlap function, and is independent of the core laser polarization. Table VI sumarizes the total relative transition moment to each jj-coupled state for the case of all lasers having parallel ($\|$) polarizations, and for the case where the core laser polarization is perpendicular ($\perp$) to that of the other three lasers.

From Table VI it is clear that the total integrated transition probability is the same, independent of the core laser polarization. The ICE model requires this, since the ionic $6s$ electron has an isotropic wave function, even when the Rydberg electron is oriented. This serves as a convenient normalization to insure that the core laser power is the same for the two polarization cases.

The final step in producing a spectrum is to create an MQDT spectrum from the calculated parameters. Since these lines are relatively broad, compared to the spacing between adjacent Rydberg states, it is important to use a multichannel model. However, none of the four states interfere with each other, either because they have different J values, or because they are coupled to independent continua. Consequently, we have used a sum of independent two-channel line shapes. Each two-channel line shape is characterized by a quantum defect δ, which is related to its binding energy relative to the excited ion as

$$W = \frac{-1}{2(n^*)^2} = \frac{-1}{2(n-\delta)^2} \tag{12}$$

and by an R matrix element which is approximately related to the state's linewidth by

TABLE VI. Relative transition probabilities to each of the jj-coupled $6p_{1/2}nf$ states from an initial $6snf\ ^1F_3$ state.

	$\lvert T_\parallel\rvert^2$	$\lvert T_\perp\rvert^2$
$(6p_{\frac{1}{2}}nf_{\frac{5}{2}})_2$	6	2
$(6p_{\frac{1}{2}}nf_{\frac{5}{2}})_3$	0	4
$(6p_{\frac{1}{2}}nf_{\frac{7}{2}})_3$	0	3
$(6p_{\frac{1}{2}}nf_{\frac{7}{2}})_4$	8	5

$$R^2 = \frac{\pi(n^*)^3\Gamma}{2}\ . \tag{13}$$

The character of the state is then spread over energy (represented by the effective quantum number n^*) as

$$A^2 = \frac{R^2}{\sin^2(\pi n^*) + R^4\cos^2(\pi n^*)}\ . \tag{14}$$

A complete spectrum is obtained by adding together the independent lines, mulitplied by their excitation weights from Table VI, and then multiplying the entire sum by the overlap function $|\langle nf|n'f\rangle|^2$, where

$$\langle nf|n'f\rangle = \frac{\sin[\pi(n* - n'^*)]}{\pi(W_n - W_{n'})}\ . \tag{15}$$

The initial n^* values for the $6snf\ ^1F_3$ states are $n^* = 13.769$ and $n^*=18.586$ for the $n=14$ and 19 states, respectively, as reported by Post, Vassen, and Hogervorst.[21]

IV. ANALYSIS AND DISCUSSION

The $6p_{1/2}nf$ states have been characterized and shown to have little variation in quantum defects, but a significant variation in scaled linewidths $[(n^*)^3\Gamma]$. This has been attributed to configuration interaction between the $6p_{1/2}nf$ and the $6p_{3/2}nf$ series. We have chosen two n values for our detailed polarization studies, n=19 ($n^*_{3/2} = 7.41$) which appears to be relatively unperturbed, and $n = 14$ ($n^*_{3/2} = 6.95$) which has the maximum scaled width, implying the maximum perturbation. In both cases we find similar behavior, although the $n = 19$ case is much closer to our calculations. The $n = 14$ case appears to have the same relative increases in all j states' linewidths relative to the $n = 19$ state, although there are small shifts in the relative positions of the J states which are readily apparent.

There is little apparent difference between the parallel and perpendicular spectra for the $6p_{1/2}nf$ excitation spectra, as has been previously noted, and as can be seen from the typical spectra shown in Figs. 3 and 4. Con-

sequently, we have used a two-step analysis method to make the differences between the parallel and perpendicular spectra more apparent. First, we have fit the $J=2,4$ spectra, since they only involve two nearly degenerate lines with fixed relative amplitudes. The second step of our analysis is to normalize both spectra to have the same integrated excitation value, and then evaluate the difference between the two spectra. (Since the $6s$ ion core is isotropic, the total excitation rate must be independent of the core laser's polarization, as shown in Table VI.)

The data shown in these figures were obtained on a single day for each n state, although the other days show the same behavior (*i.e.*, linewidths, relative positions, and asymmetry of the difference spectra). Variations in the laser power profile, and laser frequency offset, and on different days make the profile easier to fit if the days are not summed together. Fitting the difference spectra, rather than matching the fine details of each spectra, allows us to eliminate fitting errors which could result from the laser power varying over the line shape, from uncertainties about the absolute laser frequency calibration, and from nonlinearities in the laser frequency sweep. With this method, it is possible to perceive the small change in relative quantum defects which occurs because of the configuration interaction with the perturbing $6p_{3/2}7f$ state. Note that the difference spectra show reversed asymmetry, for example. Table VII shows the results of our fits to these spectra, with our calculated linewidths, to be compared to the $n=19$ states.

Figure 3 also shows calculated $6p_{1/2}19f$ spectra for the

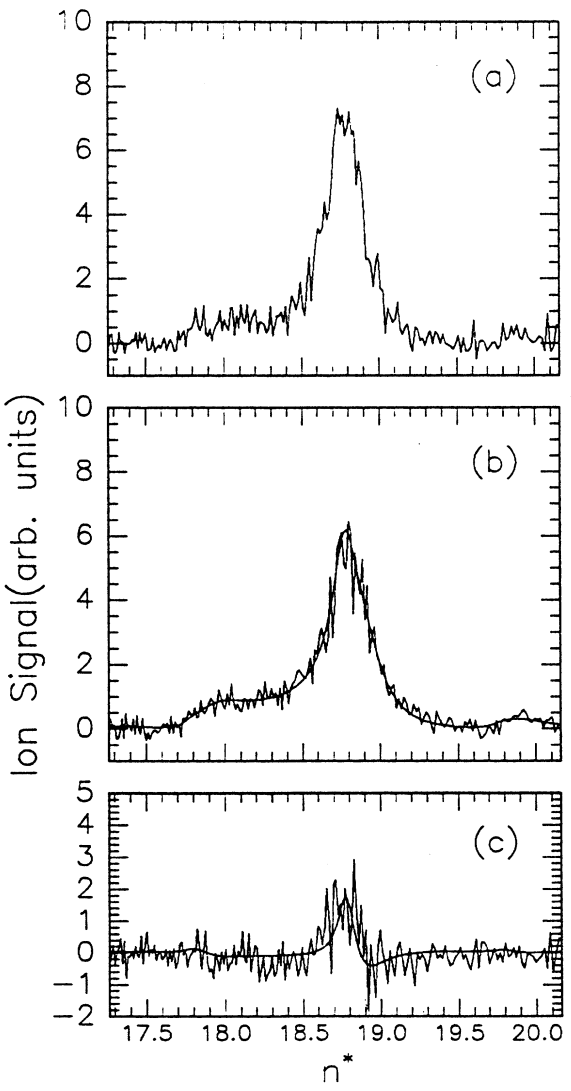

FIG. 3. Perpendicular (a), parallel (b), and difference (c) spectra for $6p_{1/2}19f$ states. Also shown in (b) and (c) are spectra constructed using our calculated linewidths.

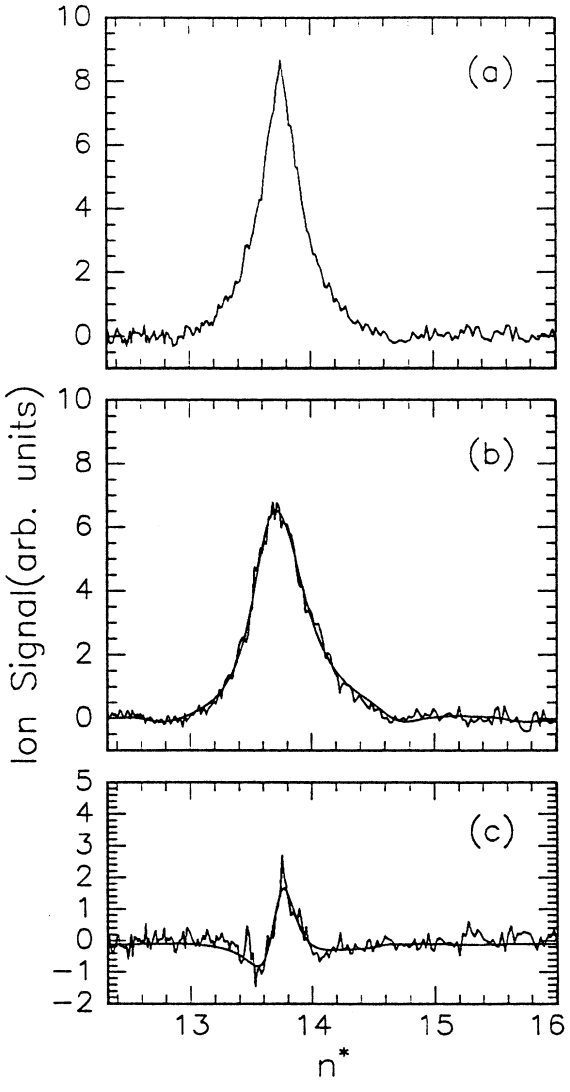

FIG. 4. Perpendicular (a), parallel (b), and difference (c) spectra for $6p_{1/2}14f$ states. Also shown in (b) and (c) are least-squares fits of the spectra.

TABLE VII. Quantum defects and linewidths of the $6p_{1/2}14f$ and $6p_{1/2}19f$ states.

J	n	δ	R^2	R^2_{calc}
2	14	0.37	0.54	
3		0.25	0.45	
3		0.25	0.45	
4		0.22	0.66	
2	19	0.22	0.33	0.29
3		0.22	0.29	0.21
3		0.22	0.29	0.33
4		0.10	0.50	0.50

$J = 2,4$ case and the difference spectra, where we have used our calculated width values and the fitted values for the quantum defects. For the difference spectra, we have used both calculated widths, but only one $J = 3$ quantum defect, forcing the two states to be degenerate. When we attempted to use two $J = 3$ states, the noise in the data forced our least-squares routine into a unreliable minimum by trying to make two narrow peaks. We believe that there is insufficient data to extract details on the differences between the two $J = 3$ states. We have not plotted the fitted spectra because the two are nearly identical in a figure, the only apparent difference is an $\approx$10% difference in the peaks heights. Overall, the agreement is excellent.

Figure 4 also shows a least-squares fit to the $J = 2,4$ spectra and to the difference spectra, where we have used only one $J = 3$ state in the fit.

In conclusion, we have shown that there are differences between the $6p_{1/2}nf$ spectra excited with different polarization, and that those differences can be used to extract meaningful information about the $J = 3$ states. These $J = 3$ states are somewhat narrower than the other states because the remnants of the LS coupling gives them a larger fraction of the $L = F$ character, which decays the slowest. We have shown that the $6p_{1/2}nf$ multiplets have are nearly degenerate, and that a simple Slater integral type of calculation can accurately reproduce their anomalously large widths.

ACKNOWLEDGMENTS

This work was supported by the National Science Foundation under Grant No. PHY88-14903.

[1] W.E. Cooke, T.F. Gallagher, S.A. Edelstein, and R.M. Hill, Phys. Rev. Lett. **41**, 178 (1978).
[2] F. Gounand, T.F. Gallagher, W. Sandner, K.A. Safinya, and R. Kachru, Phys. Rev. A **27**, 1925 (1983); O.C. Mullins, Y. Zhu, E.Y. Xu, and T.F. Gallagher, *ibid.* **32**, 2234 (1985).
[3] S.M. Jaffe, R. Kachru, H.B. van Linden van den Heuvell, and T.F. Gallagher, Phys. Rev. A **32**, 1480 (1985).
[4] C.H. Greene, Phys. Rev. A **28**, 2209 (1983); **32**, 1880 (1985).
[5] M. Aymar, Phys. Rep. **110**, 163 (1984) and references therein; M. Aymar and J.M. Lecomte, J. Phys. B **22**, 223 (1989).
[6] M.J. Seaton, Rep. Prog. Phys. **46**, 167 (1983) and references therein.
[7] U. Fano, Phys. Rev. A **2**, 353 (1970).
[8] W.E. Cooke and C.L. Cromer, Phys. Rev. A **32**, 2725 (1985).
[9] A. Giusti-Suzor and U. Fano, J. Phys. B **17**, 215 (1984).
[10] E.Y. Xu, Y. Zhu, O.P. Mullins, and T.F. Gallagher, Phys. Rev. A **33**, 2401 (1986).
[11] L.D. Van Woerkom and W.E. Cooke, Phys. Rev. Lett. **57**, 1711 (1986).
[12] R. Kachru, H.B. van Linden van den Heuvell, and T.F. Gallagher, Phys. Rev. A **31**, 700 (1985).
[13] W. Vassen, T. van de Veldt, C. Westra, E.A.J.M. Bente, and W. Hogervorst, J. Opt. Soc. Am. B **6**, 1473 (1989).
[14] R.R. Jones, C.J. Dai, and T.F. Gallagher, Phys. Rev. A **41**, 316 (1990).
[15] E.A.J.M. Bente, Ph.D. thesis, Vrije University, Amsterdam, 1989; also see E.A.J.M. Bente and W. Hogervorst, J. Phys. B **23**, 1403 (1990).
[16] U. Fano, Phys. Rev. **125**, 1866 (1961).
[17] W.E. Cooke and S.A. Bhatti, Phys. Rev. A **26**, 391 (1982).
[18] I.I. Sobelman, *Atomic Spectra and Radiative Transitions* (Springer-Verlag, New York, 1979), p.115.
[19] H.A. Bethe and E.E. Salpeter, *Quantum Mechanics of One- and Two-Electron Atoms* (Springer-Verlag, New York, 1957), p.23.
[20] R.R. Jones and T.F. Gallagher, Phys. Rev. A **38**, 2846 (1988).
[21] B.H. Post, W. Vassen, and W. Hogervorst, J. Phys. B **19**, 511 (1986).